

Received May 19, 2022, accepted June 14, 2022, date of publication June 20, 2022, date of current version June 23, 2022.

Digital Object Identifier 10.1109/ACCESS.2022.3184450

# A Comparison Between Concentrated and Distributed Massive MIMO Channels at 26 GHz in a Large Indoor Environment Using Ray-Tracing

JESÚS R. PÉREZ<sup>1</sup>, LUIS VALLE<sup>1</sup>, ÓSCAR FERNÁNDEZ<sup>1</sup>, RAFAEL P. TORRES<sup>1</sup>,  
LORENZO RUBIO<sup>2</sup>, (Senior Member, IEEE), VICENT M. RODRIGO PEÑARROCHA<sup>2</sup>,  
AND JUAN REIG<sup>2</sup>, (Senior Member, IEEE)

<sup>1</sup>Departamento de Ingeniería de Comunicaciones, Universidad de Cantabria, 39005 Santander, Spain

<sup>2</sup>Instituto de Telecomunicaciones y Aplicaciones Multimedia, Universitat Politècnica de València, 46022 Valencia, Spain

Corresponding author: Jesús R. Pérez (jesusramon.perez@unican.es)

This work was supported by the MCIN/AEI/10.13039/501100011033/ through the I+D+i Project under Grant PID2020-119173RB-C21 and Grant PID2020-119173RB-C22.

**ABSTRACT** In this paper, a comparative analysis between concentrated and distributed massive multiple-input multiple-output channels (C-mMIMO and D-mMIMO respectively), in an indoor environment using ray-tracing (RT) in the 26 GHz band is presented. The comparison is carried out in a realistic scenario consisting of a floor of a large building. The simulations emulated the up-link channel in an indoor cell in the framework of a time division duplex (TDD) - orthogonal frequency division multiplexing (TDD-OFDM) system. Both base stations, concentrated and distributed, were equipped with an array consisting of 100 antennas, and the maximum number of 20 simultaneously active users is considered. The channels are simulated using a well-tested and rigorous RT software. Using RT channel modeling, this work characterizes the up-link channels with both technologies, estimating the coherence bandwidth of the channels and analyzing the achievable capacity, assuming perfect channel state information (CSI). The results show that the D-mMIMO channel outperforms the C-mMIMO one from the point of view of their behavior in broadband as well as in terms of the obtainable capacity.

**INDEX TERMS** 5G mobile systems, channel capacity, coherence bandwidth, massive MIMO.

## I. INTRODUCTION

The use of multiple transmitting and receiving antennas, multiple-input multiple-output (MIMO), has been a revolutionary technology for increasing channel capacity. The first versions of this technology focused on point-to-point communications (PtP MIMO) considering  $Q$  transmitter antennas and  $M$  receiver antennas. These types of channels require both a relatively high signal to noise ratio (SNR) and orthogonality between sub-channels in order to make the most of the capacity gain by spatial multiplexing. One technique to compensate for the low SNR levels that can occur at the edges of the coverage area or due to obstacles inside buildings is the use of a greater number of antennas. Moreover, the orthogonality between channels can be improved by separating the antennas that make up the array. In both cases, expanding the

physical size of the array is a limitation, especially from the point of view of the user terminal (UT).

Multiuser MIMO (Mu-MIMO) introduced a different approach to using multiple spatially separated antennas at one end of the link. One of the antenna arrays is divided into  $Q$  independent antennas, where each antenna is assigned to each UT. In this approach, although the UTs do not collaborate with each other, they do allow the orthogonality between the channels to increase, thanks to the fact that the UTs are separated by several wavelengths. Furthermore, by applying beamforming techniques at the base station (BS) side, Mu-MIMO technology allows communication with multiple users simultaneously. The handicap of Mu-MIMO is that  $Q$  is of the order of  $M$ , along with the fact that the frequency division duplex (FDD) mode used is not a scalable technology [1].

A characteristic of MIMO channels is that the capacity of the channel increases with the number of antennas. The

The associate editor coordinating the review of this manuscript and approving it for publication was Zhengqing Yun<sup>1</sup>.

very large MIMO or massive MIMO (mMIMO) technology exploits this idea on a much greater scale than Mu-MIMO, incorporating tens or hundreds of antenna elements at the BS so that  $M \gg Q$ . This way, the BS can serve tens of UTs simultaneously using time division duplex (TDD) mode. Thus, the advantages of mMIMO are clear: it increases capacity through the spatial multiplexing and improves the radiated energy efficiency with a better beamforming resolution [1]. For these reasons, mMIMO is a crucial feature for the next generation mobile communication systems [1], [2].

The increase in spectral efficiency in mMIMO technology requires an increase in the number of antennas. However, the growth in the number of array elements, with a minimum separation between them of the order of a wavelength, has important physical limitations, both when building the array and its radio frequency network, and when physically installing them [3]. The use of extremely large aperture arrays (ELAA) is a promising technology that can overcome this limitation [3]. Unlike traditional concentrated massive MIMO base stations (C-mMIMO), this technology distributes a large number of antennas over an extensive area, conforming a distributed base station. This way, the whole set of BS antennas surrounds each user terminal, rather than having the UTs surrounding the BS, as occurs in the classical cellular concept. This technology joins the idea of distributed MIMO [4]–[6] and cell free networks [7]–[10] with the mMIMO concept, giving rise to the concept of distributed massive MIMO (D-mMIMO) [11]–[16]. Another advantage of D-mMIMO is that it ensures a uniformly good service everywhere for all the UTs [1] in comparison with the C-mMIMO where the UTs located at the edge of the cell experience, with a high probability, a worse service [17], [18].

The development and deployment of high data rate communication systems like 5G and beyond, requires accurate modeling of the propagation radio channel. For this reason, mMIMO channel modeling has attracted the attention of researchers in recent years, either by expanding the existing ones or by proposing new channel models [19]–[21]. The D-mMIMO channel is characterized by very different scales of fading and shadowing, which are produced in the radio channels between each UT and the spatially distributed BS array elements, which is a challenge in the characterization and modeling of the radio channel.

Ray-tracing (RT) is a site-specific channel model that uses high-frequency approaches to Maxwell's equations to characterize radio propagation in the frequency bands of current wireless systems. The RT method is well suited for the development and subsequent deployment of systems based on mMIMO technology [22]–[24]. Thanks to the use of site-specific models, RT can adequately model the non-stationarity of the channel along the antenna elements of the array or the orthogonality between columns in the channel matrix conditioned by the relative position of the active users. In addition, it can provide other geometric information, not easily acquired by measurements, such as the direction of arrival (DoA) and departure (DoD) of the multipath

components. The authors have extensive experience in developing RT-based radio propagation simulators based on a full three-dimensional implementation of geometrical optics and the uniform theory of diffraction (3D GO/UTD) [25]–[29]. This software tool has been validated with measurement campaigns for the development of wireless systems with single-input single-output (SISO) channels [25]–[28], PtP  $2 \times 2$  MIMO channels [30] and mMIMO channels [31].

In the literature, we can find different research works that carry out, by means of RT, a characterization of the C-mMIMO [32]–[35] and D-mMIMO [36] channel. Comparative studies of both channels focus, in general, on urban environments [37]–[39]. In fact, there are few publications that analyze D-mMIMO channels in indoor environments [40] and, to our best knowledge, none in medium/large indoor environments.

This work presents a comparative analysis of the performance of D-mMIMO and C-mMIMO channels in a medium/large indoor environment. In both cases, we have considered 100 antenna elements at the BS array and up to 20 simultaneously active UTs. This ratio between the number of antennas at the BS and the maximum number of UTs can be considered reasonable in indoor environments [41], [42]. Using RT channel modeling, this work characterizes the up-link (UL) channel with both technologies, estimating the coherence bandwidth ( $B_C$ ) of the channel, a fundamental parameter for analyzing the obtainable spectral efficiency, since it determines the length in the frequency domain of the coherence block [43]. In addition, the achievable channel capacity is also investigated, assuming for both mMIMO systems a perfect channel state information (CSI). The main objective is to compare C-mMIMO versus D-mMIMO channels in terms of the intrinsic structure of the channel, i.e., to analyze to what extent the channels fulfill more closely the favorable propagation condition, avoiding the effect of the power imbalance between the different UTs.

The rest of the paper is organized as follows. In section II, we briefly introduce the RT methodology, applied to obtain the channel transfer function and characterize the mMIMO channel. Section III describes the indoor environment analyzed, its geometric and electromagnetic modeling and the configuration for both types of mMIMO systems. In section IV, we present and analyze the results obtained from the RT simulations, comparing C-mMIMO and D-mMIMO in terms of wideband channel characterization and channel capacity. Finally, section V summarizes the main conclusions that can be drawn from this work.

## II. RAY-TRACING AND CHANNEL MODEL

Ray-tracing techniques based on 3D GO/UTD models can be considered a powerful and useful tool for calculating signal levels in specific radio propagation environments [25]–[27]. The radio propagation process can be represented as a set of scattering mechanisms that contribute to electromagnetic fields, such as attenuation, transmission, reflection and diffraction. Each of these mechanisms has an associated ray,

and the coupling between both transmitter and receiver antennas is obtained by the contribution of different rays, such as direct field, multiple reflections, single and double edge diffraction, along with combinations of diffraction-reflection and reflection-diffraction. The effect of the number of contributions included in the propagation can be quantified by the mean error and the standard deviation of errors [26], [27]. The use of the binary space partitioning (BSP) algorithm to implement an efficient technique that minimizes the computational cost is highly recommended.

The 3D GO/UTD model rigorously takes into account the orientation and radiation pattern of the transmit and receive antennas, as well as the polarization of the signals. The application of a ray approach to the analysis of the radio propagation process is based on the assumption of a geometrical and electromagnetic model of the environment.

A model constructed with flat facets to represent urban and indoor scenarios is highly suitable if we add some electrical parameters such as the relative dielectric constant, conductivity, the standard deviation of the surface roughness and the transmission coefficient or the wall width. The materials, and thus their electrical properties, considered to model the obstacles must be chosen in accordance with the real environment under study. Most common materials include limestone to model external walls, brick for the internal walls, wood for the doors, glass for the windows and a perfect conductor for the metallic doors.

The 3D-GO/UTD propagation model enables not only the exact estimation of the mean power value of an area of interest, but also the detailed characterization of the radio channel in local environments. By means of RT, a statistical characterization of the channel can be obtained both in broadband and in narrowband, estimating parameters that are crucial and of interest in wireless systems, such as the crossing rate per level and the mean duration of the fadings, or the mean square delay and the coherence bandwidth of the channel [26]–[28]. Information concerning the DoA and DoD of the receiver and transmitter signal, respectively is also provided to the user. This fact allows the estimation of the correlation matrix for point-to-point MIMO channels and the channel capacity in specific indoor environments [30].

From the RT results, the impulse response of the channel can be easily obtained as:

$$h(\tau) = \sum_{i=1}^N a_i \delta(\tau - \tau_i) \quad (1)$$

where  $N$  is the number of rays connecting transmitter and receiver antennas,  $a_i$  is the complex voltage induced on the antenna by each ray and  $\tau_i$  represents the arrival time of that ray. The channel transfer function is calculated as the Fourier transform of the impulse response as:

$$H(f) = F\{h(\tau)\} = \int_{-\infty}^{\infty} \sum_{i=1}^N a_i \delta(\tau - \tau_i) e^{-j2\pi f\tau} d\tau$$

$$= \sum_{i=1}^N a_i e^{-j2\pi f\tau_i} \quad (2)$$

The power delay profile can be easily obtained from the impulse response of the channel, i.e.,  $P(\tau) = |h(\tau)|^2$ . In the frequency domain, the channel can be characterized using the autocorrelation function, which is calculated as the Fourier transform of the power delay profile. Finally, a relevant broadband parameter, the channel coherence bandwidth,  $B_C$ , can be obtained as the frequency range from which the normalized autocorrelation function falls below a certain value [31], [43], [44].

Concerning the calculation of the channel capacity for a massive OFDM-MIMO system and concentrating on the UL, let us consider a unique cell system in which the BS is equipped with  $M$  antennas and there are a maximum number  $Q$  of active UTs, each one equipped with a single antenna [45]. Furthermore, several assumptions have been considered:

- The users transmit a total power  $P$ , the BS knows the channel, the UTs are not collaborating among each other and the OFDM system works with  $N_f$  sub-carriers.
- SNR is the mean signal to noise ratio at the receiver.
- $\mathbf{G}[k]$  is the channel matrix of order  $M \times Q$ .
- $\mathbf{s}[k]$  is a column vector with  $Q$  elements representing the signals transmitted from the UTs and normalized so that  $E\{\|\mathbf{s}\|^2\} = 1$ .
- $\mathbf{n}[k]$  is a complex Gaussian noise vector with i.i.d. unit variance elements.

The signal received at the BS for the  $k$ -th sub-carrier when the number of UTs is  $Q$ , is a column vector with  $M$  elements obtained as:

$$\mathbf{y}[k] = \sqrt{SNR} \mathbf{G}[k] \mathbf{s}[k] + \mathbf{n}[k]; k = 1, 2, \dots, N_f \quad (3)$$

The matrix  $\mathbf{G}$  is normalized to verify:

$$E\{\|\mathbf{G}\|_F^2\} = M \cdot Q \quad (4)$$

and is obtained from the raw channel simulations ( $\mathbf{G}^{raw}$ ) as:

$$\mathbf{G}_{M \times Q} = \mathbf{G}_{M \times Q}^{raw} \mathbf{J}_{Q \times Q} \quad (5)$$

in which  $\mathbf{J}$  is a diagonal normalization matrix of order  $Q \times Q$ . Considering one of the normalization proposals presented in [46], the elements of  $\mathbf{J}$  are given by:

$$\mathbf{j}_q = \sqrt{\frac{M}{\frac{1}{N_f} \sum_{k=1}^{N_f} |g_q^{raw}[k]|^2}}; q = 1, \dots, Q \quad (6)$$

where  $g_q^{raw}[k]$  represents the raw narrowband channel of the  $q$ -th active UT, that is, the  $q$ -th column of the raw channel matrix. The resulting normalized matrix,  $\mathbf{G}$ , can be interpreted as that associated with a system in which an ideal power control is performed, i.e., the power transmitted by the UTs is not distributed equally but rather each UT is assigned a power value so that all UTs reach the BS with the same mean power [45]. In this case, it is interesting to notice that the degradation of the channel capacity with regard to the

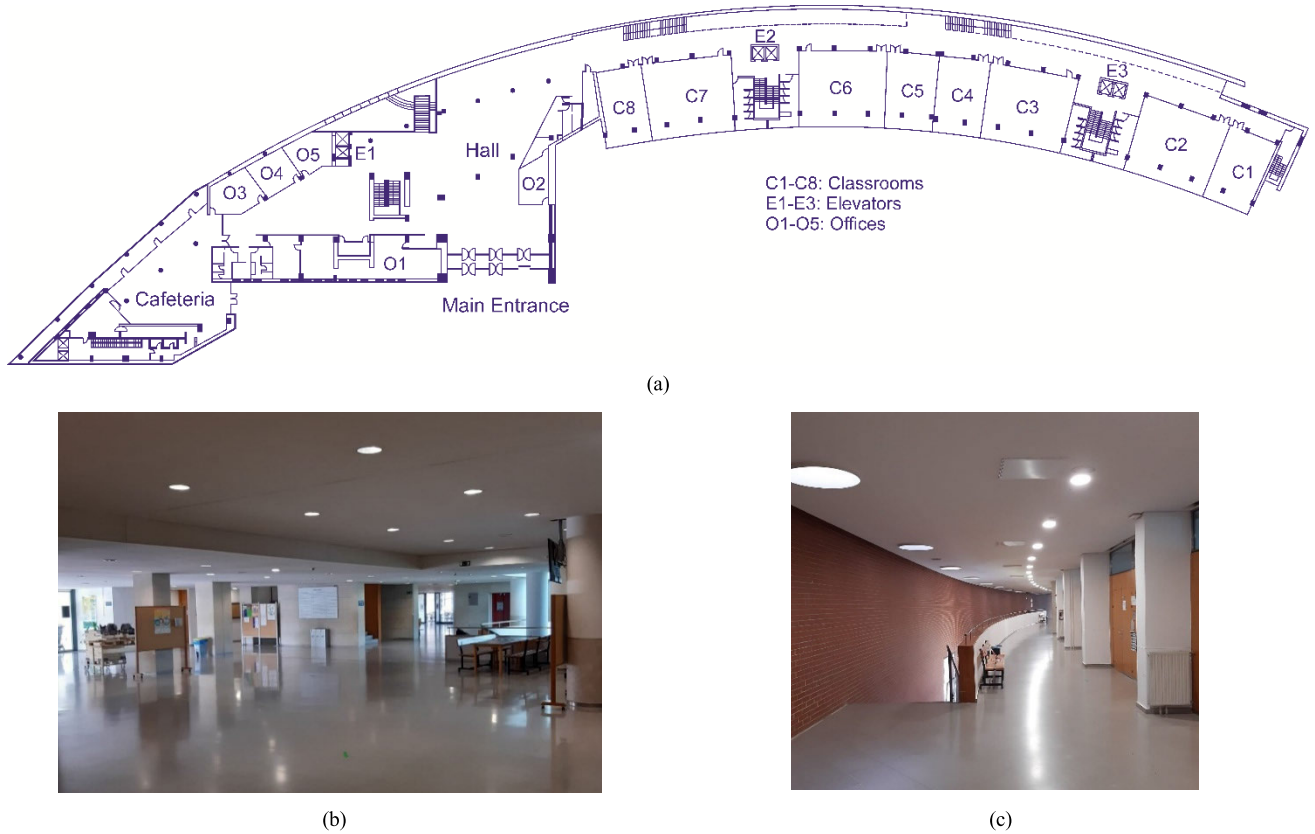


**FIGURE 1.** Details of the indoor environment (dimensions: 183 × 50 m). (a) Top view. (b) Hall of the building with a partial view of the main entrance in the upper left side. (c) Corridor that leads to the entrance of the classrooms.

reference i.i.d. Rayleigh channel depends exclusively on the orthogonality between the user sub-channels, and not on the power imbalance.

Finally, from matrix  $\mathbf{G}$ , the channel sum capacity can be obtained in order to have a metric of the goodness of the channel. Under the initial assumption that the BS knows the channel, the sum-capacity of the mMIMO UL can be calculated as:

$$C(k) = \sum_{q=1}^Q \log_2 \left( 1 + \frac{SNR}{Q} \lambda_q \right); k = 1, 2, \dots, N_f \quad (7)$$

in which  $\lambda_q$  represents the  $q$ -th eigenvalue of the  $\mathbf{G}^H \mathbf{G}$  matrix, i.e., the square of the  $q$ -th singular value of the  $\mathbf{G}$  matrix.

The capacity of the UL channel, under favourable propagation conditions, for a fixed number of transmitters  $Q$ , and as the number of receiver antennas  $M$  increases will tend asymptotically to the upper bound [2]:

$$C_b = Q \cdot \log_2 \left( 1 + \frac{M \cdot SNR}{Q} \right) \quad (8)$$

### III. ENVIRONMENT, MODELING AND SETTINGS

This section includes a description of the indoor scenario considered as reference to compare the performance of both mMIMO systems, including details of both the geometric and electromagnetic properties of the 3D model created to

accurately represent it. Furthermore, information regarding the main settings considered in the simulations, including the location of both transmitter (Tx) and receiver (Rx) antennas, the type of antennas, their height above the ground, the frequency band or the multipath contributions considered to model the propagation using RT in the simulator tool, are also summarized.

#### A. THE INDOOR ENVIRONMENT AND MODELING

The indoor environment considered in this work is shown in Fig. 1(a), and corresponds to the main floor of a very large and modern academic building at the University of Cantabria. Some particular details are also included in Figs. 1(b)-(c) to give the reader an idea of what the environment is like.

The environment houses teaching activities, including classrooms along with administrative and service areas. Furthermore, the semicircular shape of the building makes it a complex and interesting environment from a channel characterization point of view, making it possible to explore and mix up different propagation conditions.

Regarding the materials of the building, floors and ceilings are made of reinforced concrete, including ceiling boards, both the partitions as well as the main walls are made of brick; and it must be pointed out that the rear wall of the classrooms facing outdoors is entirely glazed. According to

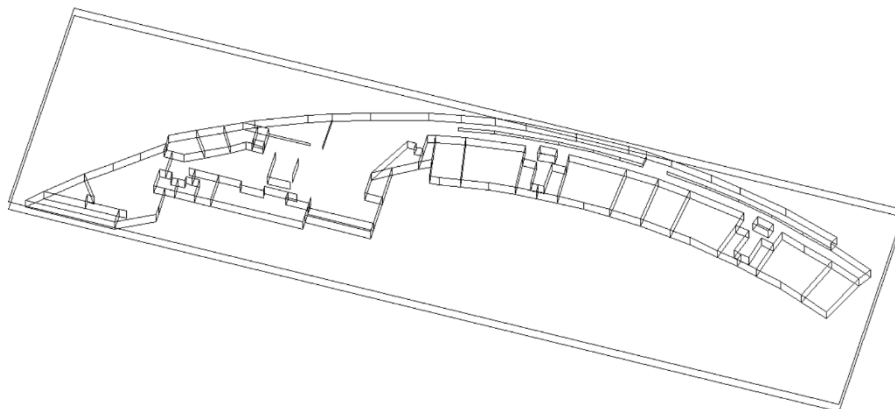


FIGURE 2. 3D model of the environment considered in the channel simulator.

TABLE 1. Material properties.

Material	$\eta'$	$\sigma$ (S/m)	Use
Brick	3.91	0.0401	Walls
Concrete	5.24	0.5908	Floor & ceiling
Glass	6.31	0.2828	Rear walls of C1-C8
Metallic surface	1	1e+7	Elevators E1-E3

such characteristics, the 3D geometric model developed and used in the channel simulator is presented in Fig. 2, and consists of 180 flat plates necessary to include the main elements of the scenario. Bearing in mind the frequency band and the potential influence of electrically large objects on the ray-tracing results, the 3D model finally considered exhibits a good balance between accuracy modeling and computational cost.

Furthermore and concerning the electromagnetic properties of any plate within the model, material electrical properties such as the real part of the relative permittivity,  $\eta'$ , and conductivity,  $\sigma$ , must be appropriately set. In this work, these parameters have been approximated using ITU frequency-dependent expressions [47]:

$$\eta' = af^b \tag{9}$$

$$\sigma = cf^d \tag{10}$$

where  $f$  is the center frequency of the band of interest in GHz, i.e., 26 GHz,  $\sigma$  is given in S/m,  $\eta'$  is dimensionless and  $a$ ,  $b$ ,  $c$  and  $d$  are constants used to characterize each material [47].

According to (9)-(10), Table 1 summarizes the material properties considered in this work to complete the model for the channel simulator, as well as their main use within the model. These values are used to calculate the transmission losses, the reflection coefficients, along with the diffraction coefficients [25], [27].

Finally, in the RT based simulations, the contribution of the direct and transmitted rays, up to the fourth reflected rays, diffracted and double diffracted rays, along with both

reflected-diffracted and diffracted-reflected rays, have been considered as the coupling mechanisms between Tx and Rx.

### B. C-mMIMO AND D-mMIMO SETTINGS

This work concentrates on the simulation and comparison of both C-mMIMO and D-mMIMO systems, considering only the UL and the 5G band n258 (26 GHz). Moreover, taking 26 GHz as the center frequency of the band, a bandwidth of 500 MHz has been considered (25.75–26.25 GHz), using a frequency sampling of 60 kHz, one of the subcarrier spacings covered for the new radio (5G NR) frame structure [48]. With such a frequency spacing, 8334 frequency tones are used to obtain the channel transfer function, i.e.,  $H(f)$  in (2), by applying the FFT to the channel impulse response, i.e.,  $h(\tau)$  in (1), obtained with the RT channel simulator.

Concerning the distribution of the Tx or potential active users, the 20 locations shown in Fig. 3(a) have been chosen, showing an almost uniform distribution over the whole floor of the building, and considering a height of the Tx antenna above the ground,  $h_{Tx}$ , of 1.5 m, in order to mimic the terminal of a user. Regarding the receiver side, 100 Rx locations have been considered for both systems, arranged taking into account the differences between C-mMIMO and D-mMIMO configurations. Focusing on C-mMIMO, the 100 antenna elements make up a uniform rectangular array (URA) ( $10 \times 10$  elements in size) lying on the YZ plane, with its center at a height,  $h_{Rx}$ , of 2.5 m above the floor, and with a uniform inter-element separation of  $0.536 \lambda$  at 26 GHz. This arrangement is shown in Fig. 3(a) labeled as Rx, and is placed between the Hall and the start of the curved corridor.

Finally, for the D-mMIMO case, the Rx antennas have been spread over the entire floor of the building, as depicted in Fig. 3(b), and fixed closed to the ceiling, 20 cm below it, at a height of 2.8 m above the ground. According to Fig. 3(b), a total of 64 Rx locations (16 rows with 4 Rx antennas each one) have been chosen on the right side of the environment giving service to classrooms C1-C8, as well as the main corridor. The remaining Rx locations have been spread in

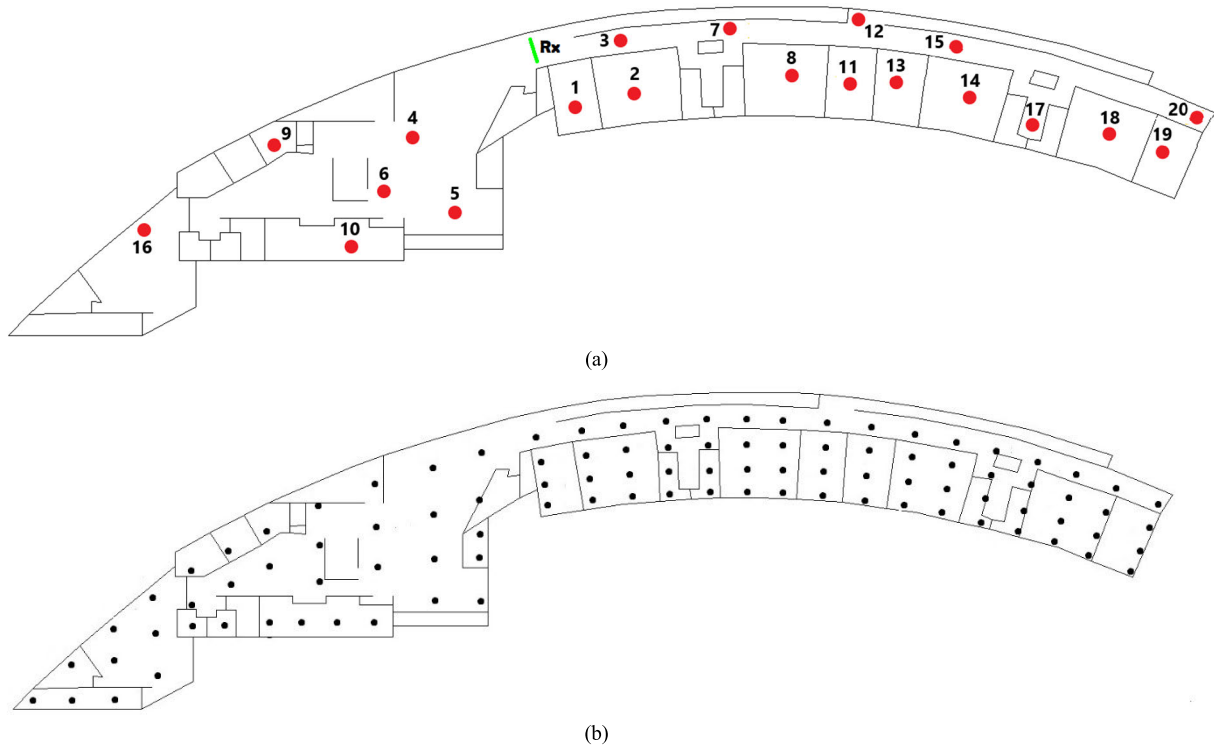


**FIGURE 3.** Transmitters and receivers locations for C-mMIMO and D-mMIMO. (a) Distribution of the 20 Tx/users on the site. Details of both location and orientation of the receiver array for the C-mMIMO case are included. (b) Distribution of the 100 Rx antennas for the D-mMIMO situation.

such a way that both service areas, including offices O1-O5, and the hall of the building can be serviced.

Concerning the antennas used in the simulations, a  $\lambda/2$  dipole has been used on the Tx side (to emulate active users in the UL) as well as on the Rx side for the C-mMIMO case. For the D-mMIMO, on the Rx side the far-field pattern of an omnidirectional ceiling mount antenna, the HG35805CUPR-NF model from L-Com, has been reproduced and used in the simulator.

The main settings considered in the simulations and outlined in this subsection for both C-mMIMO and D-mMIMO configurations, are summarized in Table 2.

#### IV. RESULTS

The comparison between both mMIMO systems, i.e., C-mMIMO and D-mMIMO, has been carried out in the indoor environment presented in the previous section. The most representative results concerning the statistical distribution of relevant wideband parameters such as the coherence bandwidth or the channel capacity, are included and discussed in the following subsections.

##### A. FREQUENCY SELECTIVITY

Broadband communication systems, in general, are strongly influenced by frequency selectivity. For the mMIMO systems, in the framework TDD-OFDM, channel access methods and the design of scheduling strategies depend on the

**TABLE 2.** Summary of C-mMIMO and D-mMIMO configuration.

Parameter		C-mMIMO	D-mMIMO
Frequency	Band	n258 (26 GHz)	
	Bandwidth	500 MHz	
	Spacing	60 kHz	
Rx array	Elements	100	
	$h_{Rx}$ (m)	2.5 (center)	2.8
	$\Delta y$ ( $\lambda$ )	0.536	NA
	$\Delta z$ ( $\lambda$ )	0.536	NA
Antenna	Tx	$\lambda/2$ dipole	
	Rx	$\lambda/2$ dipole	HG35805CUPR-NF
Average SNR at Rx		10 dB	

frequency and time duration of the coherence blocks (ChB), as discussed in the introduction [43]. The coherence bandwidth presented by the sub-channels that are established between each UT and the various antennas of the BS, whether in the concentrated or distributed case, depends on the propagation environment and the relative position between the antennas of the UT and each antenna of the array that makes up the BS. Obviously, this channel parameter is highly variable and must be described statistically. In this subsection, we make a comparison of the C-mMIMO and D-mMIMO channels in terms of the representative values and statistics

**TABLE 3. Coherence bandwidth values for 10% and 50% outage and 50, 70 and 90% correlation levels. The 20 Tx have been considered. Values expressed in MHz.**

System	$B_C$ (50%)		$B_C$ (70%)		$B_C$ (90%)	
	10%	50%	10%	50%	10%	50%
C-mMIMO	6.07	50.95	2.29	23.36	1.07	4.98
D-mMIMO	4.55	24.02	2.90	8.87	1.43	3.08

of the coherence bandwidth of the channel. As already mentioned in section II, the  $B_C$  is obtained for each sub-channel as the frequency lag in which the normalized autocorrelation function decays below certain levels, typically 0.5, 0.7 and 0.9 are considered [43].

In Fig. 4, the CDF of the coherence bandwidth values obtained when considering the whole set of 20 active Tx and comparing both mMIMO channels for 50%, 70% and 90% correlation levels, are presented. From the results, it can be inferred that for the three correlation levels both CDFs present a similar behavior. The fact that the  $B_C$  values converge for the D-mMIMO and C-mMIMO systems in the lower tail of the CDF becomes relevant. Furthermore, the convex shape of the CDFs indicates a significant dispersion of the values, as we will analyze in detail below. Finally, the results of the coherence bandwidth values achieved are also valid for the down-link due to the reciprocity of the channels in the framework of TDD.

In Table 3, some significant statistical values are presented, such as the values of the  $B_C$  for 10% and 50% outages, i.e., the median value for the 50% particular case. It can be seen that the median value is higher for the C-mMIMO system for the three correlation levels considered. However, in the case of  $B_C(70\%)$  and  $B_C(90\%)$  for a 10% outage the values are slightly higher for the D-mMIMO channel.

In order to analyze the variability of the  $B_C$  in more detail, Figs. 5-6 present box plots for both C-mMIMO and D-mMIMO channels, respectively. In this case, the  $B_C$  values of the channels that are established between each one of the 20 UTs and the 100 BS antennas are represented. In each box, the central mark indicates the median, and the bottom and top edges of the box indicate the 25th and 75th percentiles, respectively. Outside of the box fall the remaining 50 UT-Rx channels. First of all, it is clearly observed that there is a greater dispersion of values for all the UTs in the case of the D-mMIMO channel when compared to the C-mMIMO one. This is reasonable because in the case of the C-mMIMO system each UT sees the BS antennas over a relative small angular range. This implies that the sub-channels that make up the MIMO matrix have a greater similarity than in the case of the D-mMIMO system. In the latter case, each UT suffers from a very different channel to reach each BS antenna. In this case, the main contributions to the impulse response of the channel and thus the frequency autocorrelation function, changes substantially between the different sub-channels,

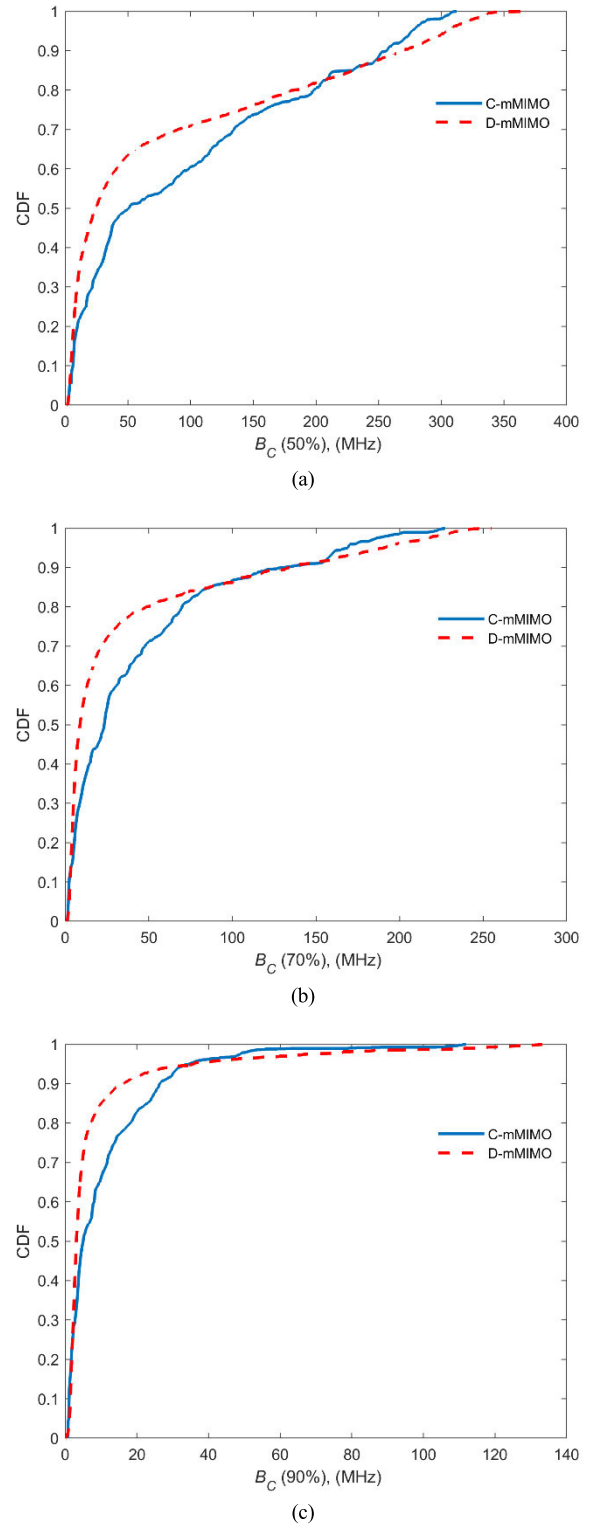
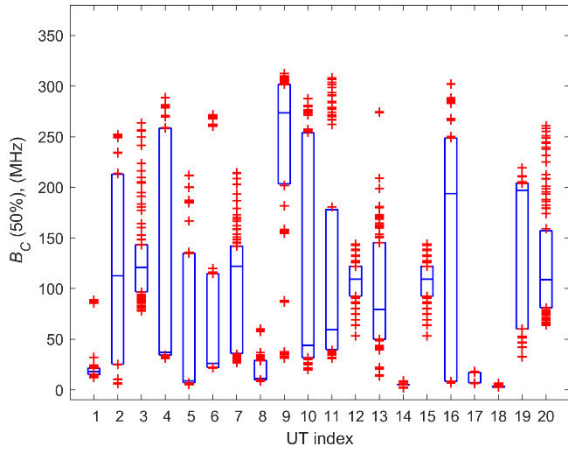
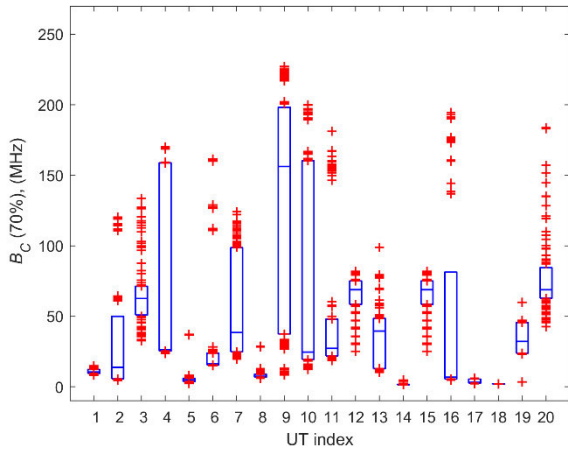


**FIGURE 4. CDF of the coherence bandwidth values obtained when considering the whole set of 20 active Tx and comparing both mMIMO systems for different correlation levels. (a) 50%. (b) 70%. (c) 90%.**

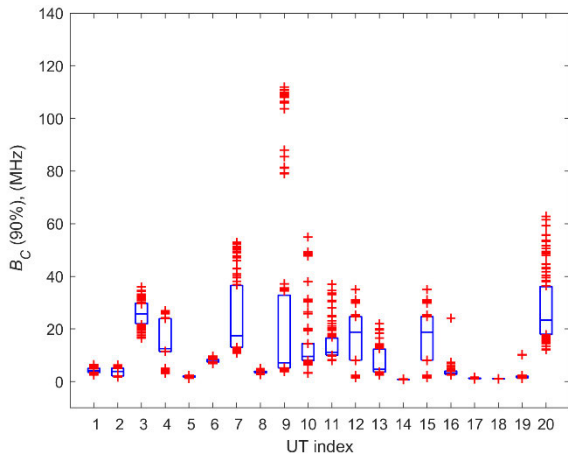
giving rise to a greater dispersion of the coherence bandwidth values. Secondly, if we compare the behavior of the 20 UTs with each other and for both systems, concentrated and distributed, we can observe that in the case of the D-mMIMO



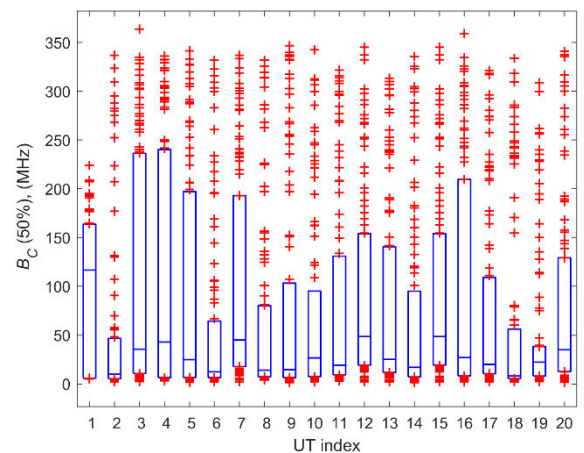
(a)



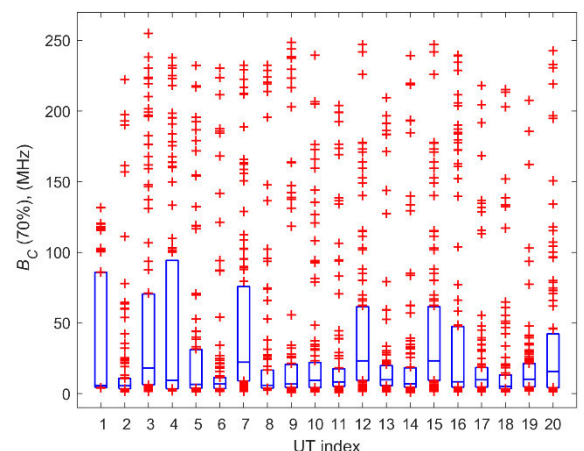
(b)



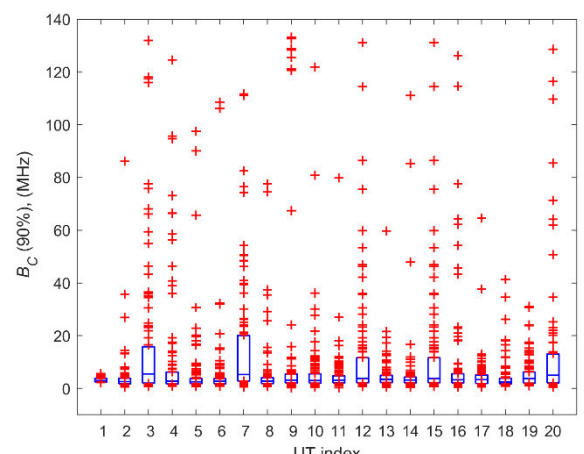
(c)



(a)



(b)



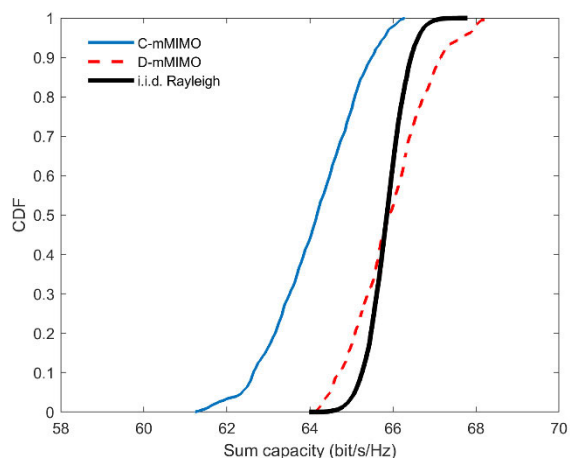
(c)

**FIGURE 5.** C-mMIMO individual coherence bandwidth values experienced by the 20 UTs and different correlation levels: (a) 50%, (b) 70% and (c) 90%.

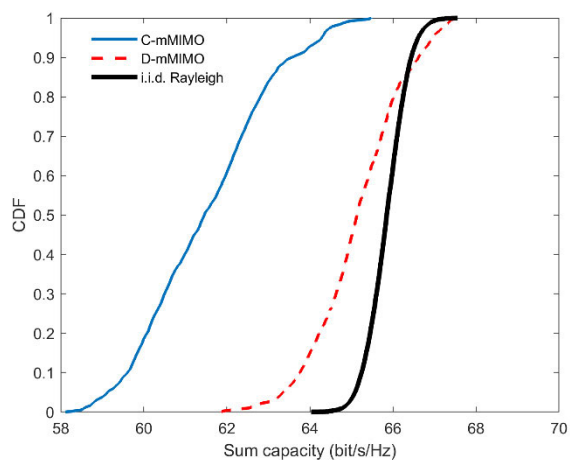
**FIGURE 6.** D-mMIMO individual coherence bandwidth values experienced by the 20 UTs and different correlation levels: (a) 50%, (b) 70% and (c) 90%.

channel, the UTs behave in a similar way. Their median values are similar, and what is also important, the bottom edge of the boxes, which indicates the 25th percentile, also

have very similar values. On the contrary, the channels of the different UTs in the C-mMIMO system present among them more dispersed values, concerning both median values as well



(a)



(b)

**FIGURE 7.** CDF of the sum capacity for C-mMIMO and D-mMIMO systems and 10 active users or Tx in two situations. (a) Dispersed Tx (Tx: 1, 3-4, 8, 10, 12, 15-17, 20). (b) Nearby Tx (Tx: 8, 11-15, 17-20).

as the percentiles. From the point of view of implementing channel-dependent scheduling strategies and antenna selection, the D-mMIMO channel performance appears to be more suitable.

**B. SUM CAPACITY**

In this subsection, we present the capacity of both UL mMIMO channels, calculated by means of (7), and considering an average SNR at the receiver array of 10 dB. Three different situations have been considered, showing the influence on the capacity of the number and distribution of the active UTs, considering 10, 15 and the whole set of 20 UTs as simultaneously active.

Let us consider first the case of 10 active users to carry out an initial comparison between both mMIMO systems taking into account the spatial distribution of the UTs in two different situations: 1) a set of 10 disperse UTs distributed throughout the entire area of interest and relatively separated from each other (Tx 1, 3-4, 8, 10, 12, 15-17, and 20), and 2) a

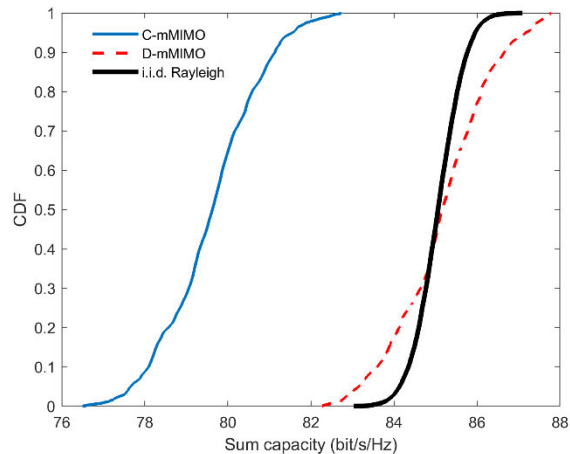


**FIGURE 8.** CDF of the sum capacity for C-mMIMO and D-mMIMO systems and 15 active users or Tx (Tx: 1-2, 4-5, 7-11, 13-16, 18-19).

set of 10 nearby UTs located next to each other and concentrated in a specific area of the building (Tx 8, 11-15, 17-20).

The cumulative distribution functions (CDFs) of the sum capacities obtained by C-mMIMO and D-mMIMO systems and for both situations, i.e., 1) and 2), are shown in Fig. 7. The CDF corresponding to an independent and identically distributed (i.i.d) Rayleigh channel is included as a reference. From the results, it is observed in terms of channel capacity that the D-mMIMO system outperforms the C-mMIMO one in both cases 1) and 2), i.e., either dispersed or nearby UTs. In addition and for both mMIMO systems, in case 1), when the transmitters are far away from each other, the capacity values obtained are greater than in 2), when the UTs are closer. As shown in Table 4, for the case of nearby users the D-mMIMO system has an outage sum capacity at 10% of approximately 4 bit/s/Hz higher than the C-mMIMO system. In the case of dispersed users, the improvement of the D-mMIMO system against C-mMIMO is smaller but still significant, 2 bit/s/Hz.

In Fig. 8, the CDFs of the sum capacity for the case of 15 active UTs are presented (Tx 1-2, 4-5, 7-11, 13-16, 18-19). In this case, it makes no sense to analyze the spatial distribution of the set of users (dispersed versus nearby UTs), because 15 is very close to the maximum number of Tx positions, 20, making it difficult to distinguish between both situations. From the numerical results summarized in Table 4, it can be observed that the outage sum capacity at 10% corresponding to the D-mMIMO channel is 5.5 bit/s/Hz greater than that obtained by the C-mMIMO system.

Finally, for the case of 20 active users, the results showing the channel sum capacity obtained can be seen in Fig. 9, and the most relevant values in Table 4. The CDF for the D-mMIMO channel shows that it equals the median value of the capacity of an i.i.d. Rayleigh channel. The difference between the sum capacity of the C-mMIMO and D-mMIMO channels widens, reaching 11 bit/s/Hz for the outage sum capacity at 10%. It is also important to note that for 20 UTs

**TABLE 4.** Representative values of the sum capacity (C) obtained for 10% and 50% outage, considering both mMIMO systems and the three sets of active users (10, 15 and 20 Tx). Values expressed in bit/s/Hz.

Number of Tx	System	C (10%)	C (50%)
10 (Nearby)	C-mMIMO	59.61	61.46
	D-mMIMO	63.76	65.13
10 (Dispersed)	C-mMIMO	62.64	64.17
	D-mMIMO	64.70	65.92
15	C-mMIMO	78.10	79.63
	D-mMIMO	83.61	85.17
20	C-mMIMO	97.23	98.83
	D-mMIMO	108.51	110.52

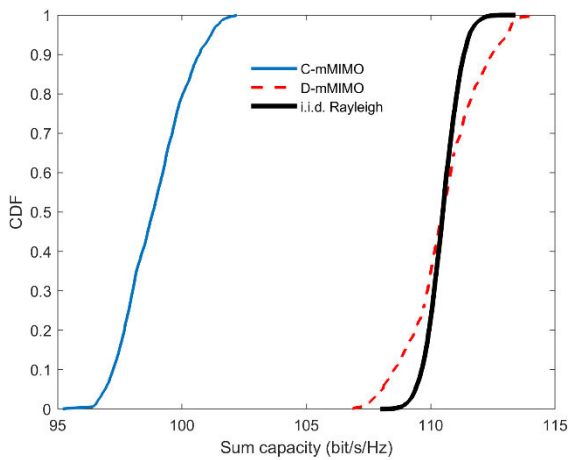


**FIGURE 9.** CDF of the sum capacity for C-mMIMO and D-mMIMO systems and considering active all the 20 users or Tx.

and 100 distributed antennas, the resulting mean capacity of the MIMO channel is close to the upper boundary of 113.5 bit/s/Hz, given by (8).

The results show a clear advantage of the D-mMIMO over the C-mMIMO channel performance in terms of capacity. For the correct interpretation of these results, it is important to highlight that the normalization carried out to calculate the capacity (6) can be interpreted in such a way that both mMIMO systems perform an ideal power control. In this sense, the average SNR at each receiver array is the same, 10 dB in our case, and thus, the degradation of the channel capacity with regard to the reference i.i.d. Rayleigh channel depends exclusively on the orthogonality between the user sub-channels, and not on the power imbalance. The widespread spatial distribution of the antennas on the distributed BS side provides very different channels between each UT and each one of the BS antennas; thus, the elements in the  $\mathbf{G}$  matrix present a different and independent fading that favors the orthogonality between them.

It is also of interest to analyze how the channel mean sum capacity increases when the number of active users grows,

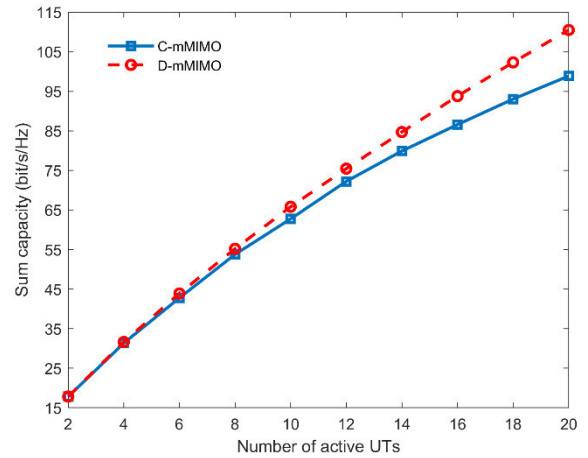


**FIGURE 10.** Sum capacity values achieved in terms of the number active UTs. Active UTs have been grouped ranging from 2 to 20 in steps of 2.

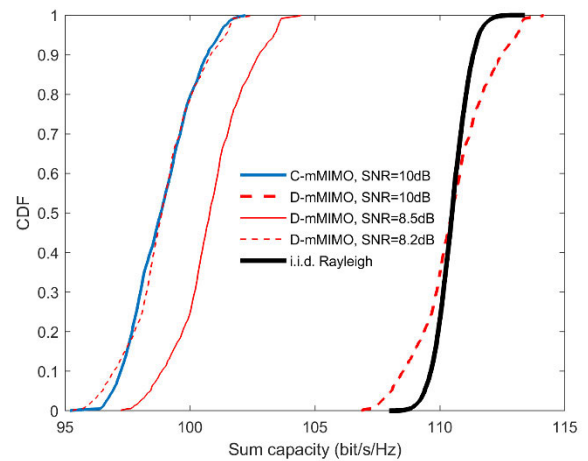


**FIGURE 11.** Analysis of the reduction of the SNR achieved with the D-mMIMO system, considering active the 20 UTs.

and to compare both C-mMIMO and D-mMIMO channels in this sense. In Fig. 10 the mean sum capacity values achieved in terms of the number active UTs are presented; the results show the influence of the number of active UTs on the achievable sum capacity. Active UTs have been grouped ranging from 2 to 20 in steps of 2. For each set of UTs it is shown the mean capacity obtained for all the possible combinations of users in order to average the effect of the concrete position of the UTs. It can be observed how for the D-mMIMO system the mean sum capacity grows faster as the number of active UTs increases than for the C-mMIMO one. This effect reinforces the conclusion that the macrodiversity due to widespread spatial distribution of the antennas on the distributed BS, causes the elements in the  $\mathbf{G}$  matrix present a different and independent fading that favors the orthogonality between them and, consequently, a greater spatial multiplexing capacity than the concentrated system.

Finally, and to quantify in terms of SNR the improvement of the D-mMIMO system, let us consider investigating the reduction in the mean SNR required in the D-mMIMO system

to achieve the same sum capacity values as those obtained by the C-mMIMO channel. According to the results presented in Fig. 11, the D-mMIMO channel leads to a reduction of 1.8 dB in the required mean SNR, a significant improvement that demonstrates for the case of study that the D-mMIMO channel outperforms the C-mMIMO one.

## V. CONCLUSION

In this paper, a comparative analysis based on RT modeling between C-mMIMO and D-mMIMO radio channels in a large indoor environment has been presented. The analysis concentrates on the simulation and comparison of both C-mMIMO and D-mMIMO systems, considering the up-link (UL) and the 5G band n258 (26 GHz). To evaluate the suitability of both concentrated and distributed channels, two of the fundamental parameters that determine the spectral efficiency achievable by a mMIMO system are analyzed: the coherence bandwidth of the channel and the capacity.

Analyzing the cell as a whole, it is observed that, in the case of  $B_C$  (70%) and  $B_C$  (90%) for a 10% outage (one of the most interesting statistical figures), the values are slightly higher for the D-mMIMO channel; reaching the value of 0.6 MHz for the case of  $B_C$  (70%) and 20 active users.

When considering how the  $B_C$  behaves for the different UTs, i.e., the  $B_C$  values of the channels that are established between each one of the 20 UTs and the 100 BS antennas, it is clearly observed that there is a greater dispersion of values for all the UTs in the case of the D-mMIMO channel. Nevertheless, if we compare the behavior of the 20 UTs with each other and for both systems, concentrated and distributed, we can observe that in the case of the D-mMIMO channel, the UTs behave in a similar and homogeneous way. This last feature can make the D-mMIMO system more suitable from the point of view of implementing channel-dependent scheduling strategies and antenna selection strategies.

Concerning the capacity of the channel, we can state that the D-mMIMO clearly outperforms the C-mMIMO channel in all cases. For the case of 20 active UTs, the CDF for the D-mMIMO channel shows that it equals the median value of the capacity of an i.i.d. Rayleigh channel. The difference between the sum capacity of the C-mMIMO and D-mMIMO channels reaches 11 bit/s/Hz for the outage sum capacity at 10%. It is also important to note that for 20 UTs and 100 distributed antennas, the resulting mean capacity of the MIMO channel is close to the upper boundary of 113.5 bit/s/Hz.

Finally, if we consider the spatial distribution of users, it is concluded that the D-mMIMO system is also more capable than the C-mMIMO of distinguishing and offering greater capacity to users when they are located next to each other and concentrated in a specific area of the building.

## REFERENCES

- [1] E. G. Larsson, O. Edfors, F. Tufvesson, and T. L. Marzetta, "Massive MIMO for next generation wireless systems," *IEEE Commun. Mag.*, vol. 52, no. 2, pp. 186–195, Feb. 2014, doi: 10.1109/MCOM.2014.6736761.
- [2] F. Rusek, D. Persson, B. K. Lau, E. G. Larsson, T. L. Marzetta, O. Edfors, and F. Tufvesson, "Scaling up MIMO: Opportunities and challenges with very large arrays," *IEEE Signal Process. Mag.*, vol. 30, no. 1, pp. 40–60, Jan. 2013, doi: 10.1109/MSP.2011.2178495.
- [3] E. Björnson, L. Sanguinetti, H. Wymeersch, J. Hoydis, and T. L. Marzetta, "Massive MIMO is a reality—What is next?" *Digit. Signal Process.*, vol. 94, pp. 3–20, Nov. 2019, doi: 10.1016/j.dsp.2019.06.007.
- [4] M. V. Clark, T. M. Willis, L. J. Greenstein, A. J. Rustako, V. Erceg, and R. S. Roman, "Distributed versus centralized antenna arrays in broadband wireless networks," in *Proc. IEEE VTS 53rd Veh. Technol. Conf.*, vol. 1, May 2001, pp. 33–37, doi: 10.1109/VETECS.2001.944798.
- [5] S. Shamai (Shitz) and B. M. Zaidel, "Enhancing the cellular downlink capacity via co-processing at the transmitting end," in *Proc. IEEE VTS 53rd Veh. Technol. Conf.*, vol. 3, May 2001, pp. 1745–1749, doi: 10.1109/VETECS.2001.944993.
- [6] S. Zhou, M. Zhao, X. Xu, J. Wang, and Y. Yao, "Distributed wireless communication system: A new architecture for future public wireless access," *IEEE Commun. Mag.*, vol. 41, no. 3, pp. 108–113, Mar. 2003, doi: 10.1109/MCOM.2003.1186553.
- [7] H. Q. Ngo, A. Ashikhmin, H. Yang, E. G. Larsson, and T. L. Marzetta, "Cell-free massive MIMO versus small cells," *IEEE Trans. Wireless Commun.*, vol. 16, no. 3, pp. 1834–1850, Mar. 2017, doi: 10.1109/TWC.2017.2655515.
- [8] E. Nayebi, A. Ashikhmin, T. L. Marzetta, H. Yang, and B. D. Rao, "Precoding and power optimization in cell-free massive MIMO systems," *IEEE Trans. Wireless Commun.*, vol. 16, no. 7, pp. 4445–4459, Jul. 2017, doi: 10.1109/TWC.2017.2698449.
- [9] E. Björnson and L. Sanguinetti, "Making cell-free massive MIMO competitive with MMSE processing and centralized implementation," *IEEE Trans. Wireless Commun.*, vol. 19, no. 1, pp. 77–90, Jan. 2020, doi: 10.1109/TWC.2019.2941478.
- [10] X. You, D. Wang, and J. Wang, *Distributed MIMO and Cell-Free Mobile Communication*. Singapore: Springer, 2021.
- [11] L. Dai, "A comparative study on uplink sum capacity with co-located and distributed antennas," *IEEE J. Sel. Areas Commun.*, vol. 29, no. 6, pp. 1200–1213, Jun. 2011, doi: 10.1109/JSAC.2011.110608.
- [12] H. Zhang and H. Dai, "On the capacity of distributed MIMO systems," in *Proc. Conf. Inf. Sci. Syst.*, Princeton, NJ, USA, Mar. 2004, p. 1.5.
- [13] H. Dai, "Distributed versus co-located MIMO systems with correlated fading and shadowing," in *Proc. IEEE Int. Conf. Acoust. Speed Signal Process.*, Toulouse, France, May 2006, pp. 561–564, doi: 10.1109/ICASSP.2006.1661030.
- [14] H. Dai, H. Zhang, and Q. Zhou, "Some analysis in distributed MIMO systems," *J. Commun.*, vol. 2, no. 3, pp. 43–50, May 2007, doi: 10.4304/jcm.2.3.43-50.
- [15] A. Amiri, M. Angjelichinoski, E. de Carvalho, and R. W. Heath, "Extremely large aperture massive MIMO: Low complexity receiver architectures," in *Proc. IEEE Globecom Workshops (GC Wkshps)*, Abu Dhabi, UAE, Dec. 2018, pp. 1–6, doi: 10.1109/GLOCOMW.2018.8644126.
- [16] H. B. Almelah and K. A. Hamdi, "Spectral efficiency of distributed large-scale MIMO systems with ZF receivers," *IEEE Trans. Veh. Technol.*, vol. 66, no. 6, pp. 4834–4844, Jun. 2017, doi: 10.1109/TVT.2016.2616173.
- [17] G. Interdonato, E. Björnson, H. Q. Ngo, P. Frenger, and E. G. Larsson, "Ubiquitous cell-free massive MIMO communications," *EURASIP J. Wireless Commun. Netw.*, vol. 2019, no. 1, pp. 1–13, Aug. 2019, doi: 10.1186/s13638-019-1507-0.
- [18] T. Choi, P. Luo, A. Ramesh, and A. F. Molisch, "Co-located vs distributed vs semi-distributed MIMO: Measurement-based evaluation," in *Proc. 54th Asilomar Conf. Signals, Syst., Comput.*, Nov. 2020, pp. 836–841, doi: 10.1109/IEEECONF51394.2020.9443568.
- [19] J. Flordelis, X. Li, O. Edfors, and F. Tufvesson, "Massive MIMO extensions to the COST 2100 channel model: Modeling and validation," *IEEE Trans. Wireless Commun.*, vol. 19, no. 1, pp. 380–394, Jan. 2020, doi: 10.1109/TWC.2019.2945531.
- [20] A. Ghazal, Y. Yuan, C. Wang, Y. Zhang, Q. Yao, H. Zhou, and W. Duan, "A non-stationary IMT-advanced MIMO channel model for high-mobility wireless communication systems," *IEEE Trans. Wireless Commun.*, vol. 16, no. 4, pp. 2057–2068, Apr. 2017, doi: 10.1109/TWC.2016.2628795.
- [21] S. Jaekel, L. Raschkowski, K. Börner, and L. Thiele, "QuaDRiGa: A 3-D multi-cell channel model with time evolution for enabling virtual field trials," *IEEE Trans. Antennas Propag.*, vol. 62, no. 6, pp. 3242–3256, Jun. 2014, doi: 10.1109/TAP.2014.2310220.

- [22] D. He, B. Ai, K. Guan, L. Wang, Z. Zhong, and T. Kürner, "The design and applications of high-performance ray-tracing simulation platform for 5G and beyond wireless communications: A tutorial," *IEEE Commun. Surveys Tuts.*, vol. 21, no. 1, pp. 10–27, 1st Quart., 2019, doi: [10.1109/COMST.2018.2865724](https://doi.org/10.1109/COMST.2018.2865724).
- [23] M. Z. Aslam, Y. Corre, E. Björnson, and E. G. Larsson, "Large-scale massive MIMO network evaluation using ray-based deterministic simulations," in *Proc. IEEE 29th Annu. Int. Symp. Pers., Indoor Mobile Radio Commun. (PIMRC)*, Bologna, Italy, Sep. 2018, pp. 9–12, doi: [10.1109/PIMRC.2018.8580760](https://doi.org/10.1109/PIMRC.2018.8580760).
- [24] A. Fathy, F. Newagy, and W. R. Anis, "Performance evaluation of UWB massive MIMO channels with favorable propagation features," *IEEE Access*, vol. 7, pp. 147010–147020, 2019, doi: [10.1109/ACCESS.2019.2946335](https://doi.org/10.1109/ACCESS.2019.2946335).
- [25] R. P. Torres, L. Valle, M. Domingo, S. Loredó, and M. C. Diez, "CIN-DOOR: An engineering tool for planning and design of wireless systems in enclosed spaces," *IEEE Antennas Propag. Mag.*, vol. 41, no. 4, pp. 11–22, Aug. 1999, doi: [10.1109/74.789733](https://doi.org/10.1109/74.789733).
- [26] O. Fernandez, L. Valle, M. Domingo, and R. P. Torres, "Flexible rays," *IEEE Veh. Technol. Mag.*, vol. 3, no. 1, pp. 18–27, Mar. 2008, doi: [10.1109/MVT.2008.919412](https://doi.org/10.1109/MVT.2008.919412).
- [27] S. Loredó, L. Valle, and R. P. Torres, "Accuracy analysis of GO/UTD radio-channel modeling in indoor scenarios at 1.8 and 2.5 GHz," *IEEE Antennas Propag. Mag.*, vol. 43, no. 5, pp. 37–51, Oct. 2001, doi: [10.1109/74.979366](https://doi.org/10.1109/74.979366).
- [28] R. P. Torres, S. Loredó, L. Valle, and M. Domingo, "An accurate and efficient method based on ray-tracing for the prediction of local flat-fading statistics in picocell radio channels," *IEEE J. Sel. Areas Commun.*, vol. 19, no. 2, pp. 170–178, Feb. 2001, doi: [10.1109/49.914495](https://doi.org/10.1109/49.914495).
- [29] J. Moreno, M. Domingo, L. Valle, J. R. Lopez, R. P. Torres, and J. Basterrechea, "Design of indoor WLANs: Combination of a ray-tracing tool with the BPSO method," *IEEE Antennas Propag. Mag.*, vol. 57, no. 6, pp. 22–33, Dec. 2015, doi: [10.1109/MAP.2015.2480078](https://doi.org/10.1109/MAP.2015.2480078).
- [30] S. Loredó, A. Rodríguez-Alonso, and R. P. Torres, "Indoor MIMO channel modeling by rigorous GO/UTD-based ray tracing," *IEEE Trans. Veh. Technol.*, vol. 57, no. 2, pp. 680–692, Mar. 2008, doi: [10.1109/TVT.2007.906362](https://doi.org/10.1109/TVT.2007.906362).
- [31] L. Valle, J. R. Pérez, and R. P. Torres, "Characterisation of indoor massive MIMO channels using ray-tracing: A case study in the 3.2–4.0 GHz 5G band," *Electronics*, vol. 9, no. 8, p. 1250, Aug. 2020, doi: [10.3390/electronics9081250](https://doi.org/10.3390/electronics9081250).
- [32] S. Shikhintsov, A. Thielens, S. Aerts, L. Verloock, G. Torfs, L. Martens, P. Demeester, and W. Joseph, "Ray-tracing-based numerical assessment of the spatiotemporal duty cycle of 5G massive MIMO in an outdoor urban environment," *Appl. Sci.*, vol. 10, no. 21, p. 7631, Oct. 2020, doi: [10.3390/app10217631](https://doi.org/10.3390/app10217631).
- [33] G. Liu, J. She, W. Lu, M. Zhang, and Y. Bo, "3D deterministic ray tracing method for massive MIMO channel modelling and parameters extraction," *IET Commun.*, vol. 14, no. 18, pp. 3169–3174, Nov. 2020, doi: [10.1049/iet-com.2019.0884](https://doi.org/10.1049/iet-com.2019.0884).
- [34] C. Wang, H. Papadopoulos, K. Kitao, and T. Imai, "Ray-tracing based performance evaluation of 5G mmWave massive MIMO in hotspots," in *Proc. Int. Symp. Antennas Propag. (ISAP)*, Okinawa, Japan, Oct. 2016, pp. 608–609.
- [35] J. Yao, H. Ren, and Q. Liu, "Massive MIMO channel modeling using map-based ray tracing method," in *Proc. 7th IEEE Int. Symp. Microw., Antenna, Propag., EMC Technol. (MAPE)*, Xi'an, China, Oct. 2017, pp. 1–5, doi: [10.1109/MAPE.2017.8250781](https://doi.org/10.1109/MAPE.2017.8250781).
- [36] A. O. Kaya and H. Viswanathan, "Dense distributed massive MIMO: Precoding and power control," in *Proc. IEEE Conf. Comput. Commun., Toronto, ON, Canada, Jul. 2020*, pp. 756–763, doi: [10.1109/INFOCOM41043.2020.9155377](https://doi.org/10.1109/INFOCOM41043.2020.9155377).
- [37] D. Loschenbrand, M. Hofer, B. Rainer, and T. Zemen, "Empirical and simulated performance evaluation of distributed massive MIMO," in *Proc. 53rd Asilomar Conf. Signals, Syst., Comput.*, Pacific Grove, CA, USA, Nov. 2019, pp. 952–956, doi: [10.1109/IEEECONF44664.2019.9049062](https://doi.org/10.1109/IEEECONF44664.2019.9049062).
- [38] M. M. Taygur and T. F. Eibert, "Investigation of distributed and collocated base stations in a large urban massive MIMO scenario," in *Proc. 11th Eur. Conf. Antennas Propag. (EUCAP)*, Paris, France, Mar. 2017, pp. 1577–1581, doi: [10.23919/EuCAP.2017.7928552](https://doi.org/10.23919/EuCAP.2017.7928552).
- [39] H. T. P. da Silva, R. M. Duarte, M. S. de Alencar, and W. J. L. Queiroz, "Cell-free at millimeter wave frequency simulation using the ray tracing method," in *Proc. 14th Eur. Conf. Antennas Propag. (EuCAP)*, Copenhagen, Denmark, Mar. 2020, pp. 1–5, doi: [10.23919/EuCAP48036.2020.9135459](https://doi.org/10.23919/EuCAP48036.2020.9135459).
- [40] Y. Suzuki, T. Nishimura, T. Ohgane, Y. Ogawa, and J. Hagiwara, "A study on layouts of distributed antenna arrays in an indoor multi-user massive MIMO system," in *Proc. Int. Conf. Comput., Netw. Commun. (ICNC)*, Honolulu, HI, USA, Feb. 2019, pp. 29–33, doi: [10.1109/ICCNC.2019.8685594](https://doi.org/10.1109/ICCNC.2019.8685594).
- [41] E. Björnson, E. G. Larsson, and T. L. Marzetta, "Massive MIMO: Ten myths and one critical question," *IEEE Commun. Mag.*, vol. 54, no. 2, pp. 114–123, Feb. 2016.
- [42] J. Flordelis, F. Rusek, X. Gao, G. Dahman, O. Edfors, and F. Tufvesson, "Spatial separation of closely-located users in measured massive MIMO channels," *IEEE Access*, vol. 6, pp. 40253–40266, 2018, doi: [10.1109/ACCESS.2018.2854307](https://doi.org/10.1109/ACCESS.2018.2854307).
- [43] R. P. Torres and J. R. Pérez, "A lower bound for the coherence block length in mobile radio channels," *Electronics*, vol. 10, no. 4, p. 398, Feb. 2021, doi: [10.3390/electronics10040398](https://doi.org/10.3390/electronics10040398).
- [44] J. R. Perez, R. P. Torres, L. Rubio, J. Basterrechea, M. Domingo, V. M. R. Penarrocha, and J. Reig, "Empirical characterization of the indoor radio channel for array antenna systems in the 3 to 4 GHz frequency band," *IEEE Access*, vol. 7, pp. 94725–94736, 2019, doi: [10.1109/ACCESS.2019.2928421](https://doi.org/10.1109/ACCESS.2019.2928421).
- [45] J. R. Pérez and R. P. Torres, "On the impact of the radiation pattern of the antenna element on MU-MIMO indoor channels," *IEEE Access*, vol. 8, pp. 25459–25467, 2020, doi: [10.1109/ACCESS.2020.2970769](https://doi.org/10.1109/ACCESS.2020.2970769).
- [46] X. Gao, O. Edfors, F. Rusek, and F. Tufvesson, "Massive MIMO performance evaluation based on measured propagation data," *IEEE Trans. Wireless Commun.*, vol. 14, no. 7, pp. 3899–3911, Jul. 2015, doi: [10.1109/TWC.2015.2414413](https://doi.org/10.1109/TWC.2015.2414413).
- [47] *Effects of Building Materials and Structures on Radiowave Propagation Above About 100 MHz*, document ITU Radiowave Propagation Series Recommendation ITU-R P.2040-2, Release 2, Sep. 2021.
- [48] *NR; Physical Channels and Modulation*, document 3GPP Technical Specification TS 38.211, Release 17, Dec. 2021.



**JESÚS R. PÉREZ** received the B.Sc., M.Sc., and Ph.D. degrees in telecommunications engineering from the Universidad de Cantabria, Spain, in 1996, 1999, and 2005, respectively. He joined the Department of Communications Engineering, Universidad de Cantabria, in 1999. He was awarded a Graduate Research and a Postdoctoral Grant, in 2002 and 2006, respectively. He became an Associate Professor, in 2009. His research interests include radio propagation and measurement techniques for the experimental characterization of the radio channel, computational electromagnetics, and optimization methods.



**LUIS VALLE** received the M.Sc. and Ph.D. degrees in physics (electronics) from the Universidad de Cantabria, Spain, in 1990 and 1996, respectively. He became an Associate Professor with the Department of Communication Engineering, Universidad de Cantabria. He is the author of several papers and conference contributions. His research interests include numerical and high frequency methods in electromagnetics applied to antennas and microwave components, radio propagation, and mobile communications.



**ÓSCAR FERNÁNDEZ** was born in Reinoso, Cantabria, Spain, in 1976. He received the degree in telecommunications engineering and the Ph.D. degree from the Universidad de Cantabria, in 2001 and 2007, respectively. In 2002, he joined the Department of Communication Engineering, Universidad de Cantabria, where he has worked on several research projects related to radio channel characterization and metamaterials. In 2008, he became an Associate Lecturer in electronics and an Assistant Professor in RF and microwave, in 2018. His current research interests include numerical methods in electromagnetism, chiral metamaterials characterization at microwave frequencies, microwave measurements, and radio channel characterization.



**RAFAEL P. TORRES** received the M.S. degree in physics from the Universidad de Granada, Spain, in 1986, and the Ph.D. degree in telecommunications engineering from the Universidad Politécnica de Madrid (UPM), in 1990. He became an Associate Professor with the Department of Communications Engineering, Universidad de Cantabria, Spain, where he is currently a Full Professor in signal processing and communications engineering. His fundamental lines of research have been

development of numerical methods for the analysis and design of antennas, application of high frequency techniques for simulation and analysis of the radar section, and the design of radar systems. From the end of the 90's, his research focuses on the study, modeling and measurement of the radio channel and the analysis of its impact on mobile and wireless communications systems. His main achievements focus on the development of ray-tracing methods to simulate the radio channel in complex propagation environments, on the experimental characterization of the channel, both SISO and MIMO, and on the development of space-time coding techniques.



**LORENZO RUBIO** (Senior Member, IEEE) received the degree in telecommunication engineering and the Ph.D. degree from the Universitat Politècnica de València (UPV), Spain, in 1996 and 2004, respectively. In 1996, he joined the Communications Department, UPV, where he is currently a Full Professor in wireless and radio communications. His current research interests include wireless communications, radiowave propagation, measurement and mobile time-varying channels modeling in vehicular applications, UWB communication systems, multiple-input and multiple-output (MIMO) systems, equalization techniques in digital wireless systems, and mmWave propagation.



**VICENT M. RODRIGO PEÑARROCHA** was born in Valencia, Spain, in 1966. He received the M.S. degree in telecommunications engineering from the Universidad Politécnica de Madrid, Spain, in 1990, and the Ph.D. degree in telecommunications engineering from the Universitat Politècnica de València, Spain, in 2003. He joined the Departamento de Comunicaciones, Universitat Politècnica de València, in 1991, as a Lecturer. His current research interests include radiowave propagation,

antenna measurements, instrumentation, virtual instrumentation, and laboratories and any educational activity.



**JUAN REIG** (Senior Member, IEEE) was born in Alcoy, Spain, in 1969. He received the M.S. and Ph.D. degrees in telecommunications engineering from the Universitat Politècnica de València, Spain, in 1993 and 2000, respectively. He has been a Faculty Member with the Department of Communications, Universitat Politècnica de València, since 1994, where he is currently an Associate Professor in telecommunication engineering. His research interests, include fading theory, diversity,

ultra-wide band systems, and vehicular communications in V2V and V2I networks.

...